CRYSTAL GROWTH & DESIGN

Article

pubs.acs.org/crystal

# Generation and Characterization of Standardized Forms of Trehalose Dihydrate and Their Associated Solid-State Behavior

Bahijja T. Raimi-Abraham,[§] Jonathan G. Moffat,[†] Peter S. Belton,[‡] Susan A. Barker,[§] and Duncan Q. M. Craig*[,§]

[§]UCL School of Pharmacy, 29-39 Brunswick Square, London, WC1N 1AX, United Kingdom

[†]Oxford Instruments, Tubney Woods, Abingdon, Oxfordshire OX13 5QX, United Kingdom

[‡]School of Chemistry, University of East Anglia, Norwich Research Park, Norwich, NR4 7TJ, United Kingdom

Supporting Information

**ABSTRACT:** Trehalose dihydrate is a nonreducing disaccharide which has generated great interest in the food and pharmaceutical industries. However, it is well recognized that considerable batch to batch variation exists for supposedly identical samples, particularly in terms of the thermal response. In this investigation, two standardized forms of trehalose dihydrate were generated using two distinct crystallization pathways. The two batches were characterized using scanning electron microscopy, X-ray powder diffraction, and FTIR. The thermal responses of the two forms were then studied using modulated temperature differential scanning calorimetry (MTDSC) and thermogravimetric analysis (TGA). In particular, we describe the technique of quasi-isothermal MTDSC as a means of studying the change in equilibrium heat capacity as a function of temperature. Finally, variable temperature FTIR was utilized to assess the change in bonding configuration as a function of temperature. SEM revealed significant differences in the continuity and grain structure of the two batches. The TGA, MTDSC, and quasi-isothermal MTDSC studies all indicated significant differences in the thermal response and water loss profile. This was confirmed using variable temperature FTIR which indicated differences in bond reconfiguration as a function of temperature. We ascribe these differences to variations in the route by which water may leave the structure, possibly associated with grain size. The study has therefore demonstrated that chemically identical dihydrate forms may show significant differences in thermal response. We believe that this may assist in interpreting and hence controlling interbatch variation for this material.

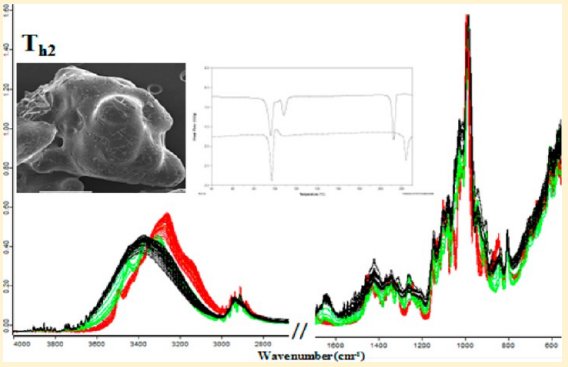


## INTRODUCTION

α,α-Trehalose dihydrate (α-D-glucopyranosyl, α-D-glucopyranoside) is a nonreducing disaccharide, consisting of two α,α units of glucopyranose linked together by an α,α-1↔1-glycosidic linkage. Water and trehalose molecules are held together within the crystal structure of this sugar hydrate by a complex hydrogen bond arrangement, whereby hydroxyl groups of trehalose molecules act as both bond donor and acceptor in the hydrogen bond network.[1] On an industrial scale, trehalose is mainly prepared by extraction from the yeast *Saccharomyces cerevisiae*, also known as Brewer's yeast. Both the food and pharmaceutical industries have a great interest in the crystalline forms of trehalose due to the use of this material as an excipient, particularly for the preservation of proteins and biological materials on processing.[2]

Trehalose exists in several crystalline, anhydrous, and amorphous forms, with the interplay between these forms being the subject of considerable study and debate. A stable crystalline anhydrous form ($T_\beta$) and an unstable crystalline anhydrous form ($T_\alpha$) were first identified.[3] The unstable crystalline anhydrous form, $T_\alpha$, is an isomorph desolvate of the stable dihydrate generated by gentle dehydration.[3] The dihydrate and $T_\alpha$ share a reversible relationship, as when $T_\alpha$ is exposed to moisture it readily reverts back to the dihydrate. Further anhydrous polymorphic forms generated from trehalose dihydrate ($T_k$)[4] and $T_\varepsilon$[5] may also exist. A crystalline form ($T_\gamma$) has also been identified,[6] which is reported to be a "transient" crystalline metastable form of trehalose. This form is thought to comprise an anhydrous shell ($T_\beta$) and a dihydrate core on a particulate basis.[7] Finally, a new solid form of trehalose has recently been identified and characterized ($T_\delta$).[8] This metastable form is generated from dehydration of the dihydrate at or below 100 °C. It is generated concurrently with ($T_\alpha$) and an amorphous form of trehalose.

Amorphous trehalose exists with a reported glass transition temperature ($T_g$) of ca. 120 °C. De Giacomo[9] proposed the existence of two amorphous phases referred to as $T_{am1}$ and $T_{am2}$. $T_{am2}$ is a noncrystallizable amorphous phase said to be the

Received: April 10, 2014
Revised: July 9, 2014
Published: August 1, 2014

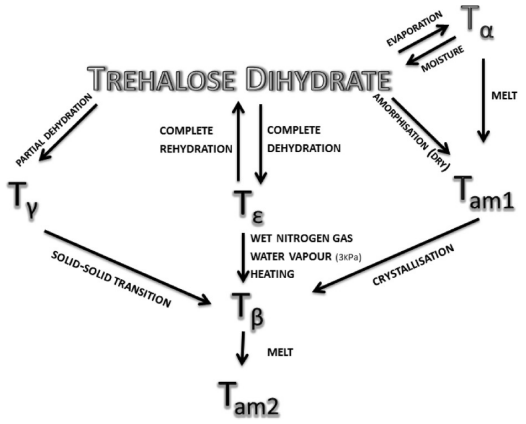


**Figure 1.** Schematic of trehalose crystalline anhydrous, hydrous, and amorphous forms, showing the interconversion between each form (adapted from Sussich et al.[10]).[3−6,9]

undercooled liquid obtained from the melt of $T_\beta$, while $T_{am1}$, a crystallizable amorphous phase, is said to be generated from the melt of $T_\alpha$. Figure 1 is a proposed schematic of trehalose crystalline anhydrous, hydrous, and amorphous forms, showing the interconversion between each form.[3−6,9]

There is uncertainty as to how the physical (in particular thermal) and interconversion properties of trehalose correlate to its bioprotective properties. Reported thermal transitions of trehalose dihydrate appear to be dependent on confinement conditions,[10] including DSC pan type (closed pan,[11] pinholed,[12] and open-pan (with and without vacuum)[11,13]) and particle size.[14,15]

Depending on experimental conditions, the observed thermal response of trehalose dihydrate can give rise to the identification of an amorphous phase; one, two, or three endotherms; and/or a crystallization exotherm. In experiments where three endotherms have been observed, for example, in a study by McGarvey et al.,[12] the first two low temperature endotherms have been attributed to the initial partial dehydration of the dihydrate resulting in a mixture of the $T_\gamma$ form and the stable anhydrate ($T_\beta$), then subsequent further dehydration of $T_\gamma$ resulting in the full formation of $T_\beta$, which then melts at ca. 210 °C. Three endotherms have also been observed in a study by Taylor and York,[14] where the first endotherm was ascribed to loss of water from the crystal lattice, the second to the melt of the $T_\alpha$ (isomorph desolvate of the stable dihydrate produced after the dehydration of the dihydrate), and the third endotherm to the melt of the stable anhydrate $T_\beta$ (formed ca. 160−180 °C but not always detectable in DSC studies). Macdonald and Johari[16] observed a single endotherm seen between 40 and 160 °C and attributed this endotherm to several processes involving the decomposition of the dihydrate crystal resulting in molecular rearrangement, leading to the formation of the stable anhydrate followed by the reorganization of the molecules to an anhydrous form of trehalose.

Along with the above inconsistencies in observed thermal responses, it is well-known within the field that there is a significant issue with batch to batch variation with material obtained from different suppliers. This has been explored by Armstrong et al.[17] who studied three different $\alpha,\alpha$-trehalose dihydrate batches. Differences were identified in DSC traces at 10 °C/min; one batch exhibited a recrystallization exotherm at 170 °C which was absent in the other two batches and two out of the three batches saw a melting endotherm at ca. 215 °C.[17] Polymorphism was not identified using X-ray powder diffraction techniques. Their results showed that while sample presentation and experimental conditions can influence the thermal response, the sample origin may also have an effect on the crystal texture and consequently the observed thermal response, which may persist after subsequent handling and processing. However, this remains an issue whereby further work would undoubtedly be of both scientific and practical value, not least because little published work is available on the subject.

In this study, we attempt to understand the variations in observed thermal transitions of trehalose dihydrate by preparing two batches via well-defined crystallization processes. Both samples were characterized using thermal and spectroscopic techniques. In particular, we explore the use of quasi-isothermal modulated temperature differential scanning calorimetry (quasi-isothermal MTDSC), a variant of modulated temperature DSC (MTDSC) whereby a sample is modulated at a series of defined temperatures for defined periods of time. This technique was developed by Wunderlich et al.[18] and has been used to characterize thermal transitions without the influence of heating rate,[19−26] including the study of polymorphic forms.[21,22,27] By using these thermal and spectroscopic techniques in conjunction, we intend to identify the characteristics that may be associated with variations in thermal response and as far as possible to relate them to the fundamental structure of the two batches of trehalose dihydrate.

## MATERIALS AND METHODS

**Materials.** $\alpha,\alpha$-Trehalose dihydrate (stated purity of ≥99%) and sodium chloride were both obtained from Sigma-Aldrich, Poole, U.K. Samples were prepared by two methods.

**Method I. $\alpha,\alpha$-Trehalose Dihydrate Crystals Generated By Slow Evaporation of a 46.6%w/w Saturated Solution.** Crystals were generated by preparing a saturated trehalose solution (46.6%w/w, the solubility of trehalose dihydrate at 20 °C).[28] 46.6 g of trehalose dihydrate (calculated as anhydrous) was dissolved in 100 g of distilled (filtered 0.45 μm) distilled water. The solution was left to recrystallize by slow evaporation at room temperature. For ease of referencing, these samples will now be referred to as $T_{h1}$. This method has been used successfully to generate large single trehalose dihydrate crystals.[13,29]

**Method II. $\alpha,\alpha$-Trehalose Dihydrate Crystals Generated By Exposure of Amorphous Trehalose to 75%RH at Room Temperature.** Based on preliminary water sorption studies on amorphous trehalose using dynamic vapor sorption (DVS) (data not shown), freshly prepared amorphous trehalose samples generated by spray drying from a 10% w/v aqueous trehalose solution (with a normal particle size distribution of 5−45 μm, confirmed amorphous by powder X-ray diffraction), were exposed to 75%RH (using a saturated sodium chloride solution stored at room temperature) for 12 hours to ensure full crystallization. For ease of referencing, these samples will now be referred as $T_{h2}$.

**Scanning Electron Microscopy.** Particle morphology was evaluated using a Scanning Electroscope JEOL JSM 5900LV. In order to improve conductivity, samples were coated with gold under vacuum SC7640 Gold Sputter Coater, 30 s, 2.2 kV, 25 mA, on the rotating stage, Quorum Technologies. All micrographs were taken at an acceleration voltage of 20 kV.

**Particle Size Analysis.** Particle size analysis was performed using a Sympactec laser particle sizer with a HELOS/Br detector. The liquid medium used was rapeseed oil. Two minute dispersion at 1000 rpm was imposed at the start of each experiment and then three measurements were taken with each sample monitored for 10 s. A measuring range of 0.1−875 μm was used. Data was exported and analyzed using OriginPro 9.0.0, Northampton, MA, USA.

**X-ray Powder Diffraction.** Ambient X-ray powder diffraction (XRPD) measurements were performed using a Thermo-Arl-Xtra with a Cu-X-ray tube. The X-ray tube was operated at 45 kV and 40 mA.


dx.doi.org/10.1021/cg5004885 | Cryst. Growth Des. 2014, 14, 4955−4967

Samples were lightly pressed into an aluminum sample tray using a glass slide and exposed to Cu K$\alpha$ radiation ($\lambda$ = 1.540562 nm). XRPD patterns were recorded using diffraction angles ($2\theta$) from 10° to 60° (step size, 0.01°; time per step, 0.5 s). Data was exported and analyzed using OriginPro 9.0.0.

**Attenuated Total Reflection Fourier Transform Infrared Spectroscopy.** Attenuated Total Reflection Fourier Transform Infrared spectroscopy (ATR-FTIR) measurements were performed using a Bruker IFS66/SG spectrometer. Experiments were performed using the following parameters: Resolution 4 $cm^{-1}$, scan count was 16 scans (also for background) over 4000 $cm^{-1}$ to 500 $cm^{-1}$ at 30 °C. Spectra were analyzed using Opus software version 6.0 and OriginPro 9.0.0. Variable temperature ATR-FTIR experiments were conducted using the parameters mentioned above by connecting a temperature controller to the diamond ATR top plate. Samples were heated from 30 to 198 °C with an applied heating rate of 2 °C/min and spectra were obtained at 1 min intervals. Spectral data obtained from variable temperature ATR-FTIR studies was analyzed using Pirouette Multivariate Data Analysis Software (v 4, Infometrix Inc.). All experiments were conducted in triplicate.

**Differential Scanning Calorimetry.** All differential scanning calorimetry (DSC) studies were conducted using a TA Instruments Q2000 (Newcastle, DE, U.S.) with a refrigerated cooling system attached at a dry nitrogen sample purge flow at 50 mL/min. Calibrations were performed using indium, *n*-octadecane, and tin; heat capacity constant calibration was performed using aluminum oxide TA sapphire discs at 0.5, 1, and 2 °C/min with ±0.212 °C modulation amplitude and 60 s period. All DSC experiments and calibrations were performed using a PerkinElmer 40 $\mu$L, 0.15 mm aluminum pan with an accompanying aluminum 0.05 mm lid with and without pinholes. Pans were crimped using a PerkinElmer Universal Crimper Press. Conventional DSC experiments were conducted at 0.5, 1, 2, 20, 50, and 100 °C/min. All experiments were conducted in triplicate.

Quasi-isothermal MTDSC involves the application of a series of oscillating heating signals at successive temperatures for time periods specified by the operator. This allows observation of time dependent responses as well as reducing the heating rate dependence of the response to a minimum due to the measurements being conducted under a series of near-isothermal conditions. In particular, the reversing heat flow (which is itself directly related to heat capacity) may be measured as a function of both temperature and time. In this manner, subtle and time-dependent changes in structure may be observed. Data may be presented as reversing heat flow as a function of time at a series of temperatures, or alternatively may be present as Lissajous figures[18] whereby the modulated heat flow may be plotted against the derivative modulated temperature, thereby allowing each oscillation to be visualized as an ellipse with axes representing the heat capacity and phase difference of the response. This in turn allows subtle changes in response to be visualized by superimposing successive ellipses taken during the period of isothermal study.

Experiments were conducted at a temperature modulation of ±1 °C and a period of 60 s with 2 °C increments from 80 to 160 °C, remaining isothermal at each increase for 20 min (5 min equilibration time, followed by 15 min measurement). All experiments were repeated at least twice with excellent reproducibility noted. Sample weights for all DSC experiments were 1−2 mg. All data obtained was analyzed using Universal Analysis 2000 software for Windows 2000/XP/Vista v 4.7A.

**Thermogravimetric Analysis.** Thermogravimetric analysis (TGA) experiments were performed on a TA Instruments Q5000IR (Newcastle, DE, U.S.) at a rate of 2 °C/min from 40 to 250 °C. All TGA experiments and calibrations were performed using a PerkinElmer 40 $\mu$L, 0.15 mm aluminum pan with an accompanying aluminum 0.05 mm lid with and without pinholes. The data obtained was analyzed using Universal Analysis 2000 software for Windows 2000/XP/Vista v 4.7A. All experiments were conducted in triplicate.

**Hot-Stage Microscopy.** Hot-stage microscopy experiments were conducted on a LeicaDML52 microscope with a 10× magnification lens connected to a FP5/FP52, Mettler Toledo Instruments heating stage unit and a FP90 Mettler Toledo Instruments central processor unit. Samples were heated from 25 to 250 °C at a heating rate of 2 °C/min. Studio86 Design capture software was used to record and capture thermal events in real time.

## RESULTS AND DISCUSSION

**Basic Characterization of Batches.** SEM images of both $T_{h1}$ and $T_{h2}$ are shown in Figure 2a−d, respectively.

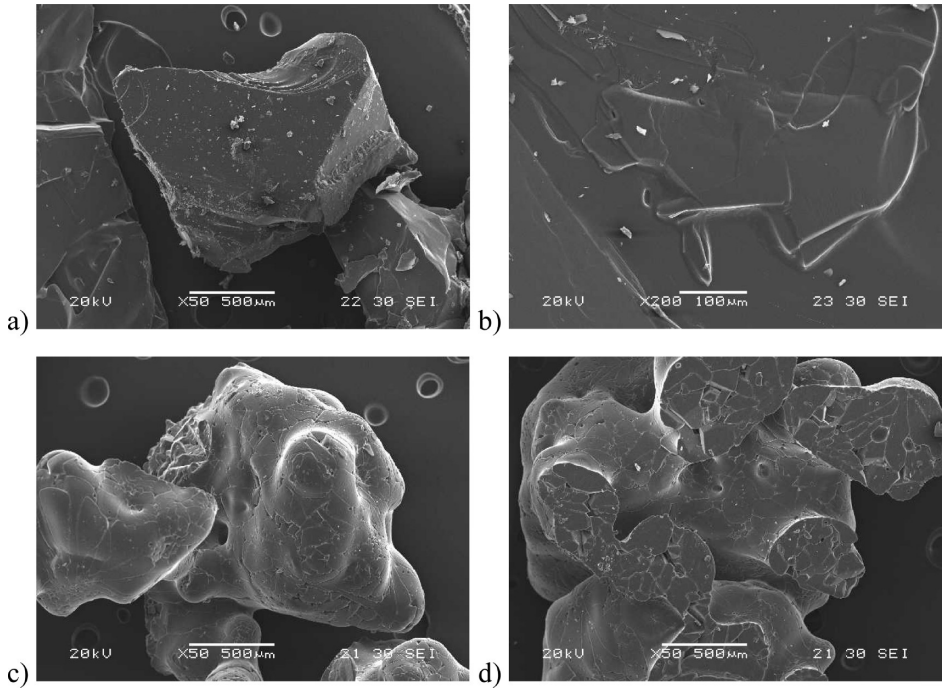


**Figure 2.** SEM images of (a) $T_{h1}$ and (c) $T_{h2}$. (b) $T_{h1}$ Cross section showing grain boundaries. (d) $T_{h2}$ Cross section showing grain boundaries. Scale bar corresponds to 500 $\mu$m (a, c, and d) and 100 $\mu$m (b).


dx.doi.org/10.1021/cg5004885 | *Cryst. Growth Des.* 2014, 14, 4955−4967

Both samples appeared to be irregularly shaped with minimal aggregation. $T_{h1}$ particles possessed angular, defined edges while $T_{h2}$ particles possessed smooth edges. $T_{h2}$ samples, however, appeared to be polycrystalline in nature, being composed of compounded crystalline structures with an approximate diameter of 50−100 $\mu$m, while $T_{h1}$ appeared to be internally continuous. We suggest that this reflects the two different production methods, with $T_{h1}$ being generated via slow crystallization to an effectively single crystal structure while $T_{h2}$ is generated via multiple nucleation from the amorphous state, leading to numerous coincident crystallites.

Particle size analysis was conducted on both samples using laser particle diffraction (Figure 3). $T_{h1}$ particles displayed

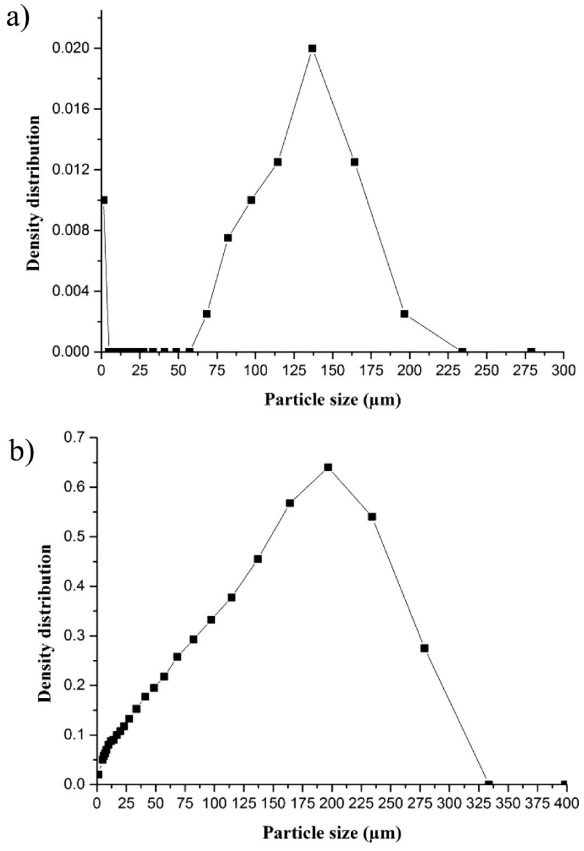


**Figure 3.** Plot showing particle size distributions of (a) $T_{h1}$ and (b) $T_{h2}$.

a bimodal distribution, with particle size ranging between 68 and 196 $\mu$m and a smaller fraction which were ca. 1.5 $\mu$m in size. $T_{h2}$ particles showed a normal distribution with particles ranging from 1.5 to 280 $\mu$m. It is noted that the two distributions are of the same order of magnitude, hence it is reasonable to suggest that the surface area/volume ratio for the two batches will be similar.

XRPD diffraction patterns for $T_{h1}$ and $T_{h2}$ (Figure 4) confirmed that both samples were crystalline. Both forms displayed characteristic diffraction peaks for trehalose dihydrate (confirmed by XRPD diffraction peaks obtained from crystal structures of trehalose dihydrate in the Cambridge Structural Database (CSD)) where peaks of 2$\theta$ 23.81° ($T_{h1}$), 23.96° ($T_{h2}$) and 15.08° ($T_{h1}$), 15.50° ($T_{h2}$) and a smaller peak of 2$\theta$ 8.69° ($T_{h1}$) and 8.92° ($T_{h2}$) were identified. Though characteristic peaks for trehalose dihydrate were identified, the diffraction patterns for $T_{h1}$ and $T_{h2}$ differed in terms of the relative

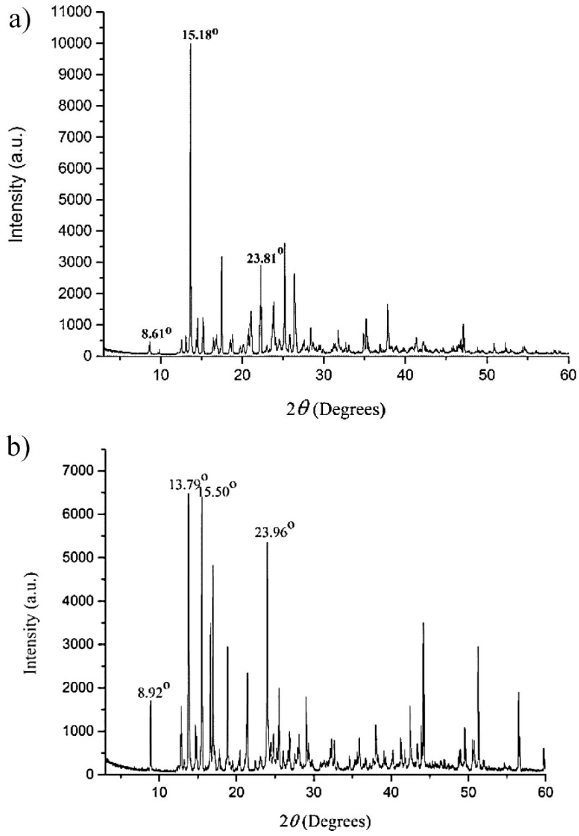


**Figure 4.** Experimental XRPD diffraction patterns for trehalose dihydrate (a) $T_{h1}$ and (b) $T_{h2}$.

intensity of the peaks. Possible explanations for the differences in diffraction patterns for both samples may be as a result of their differences in crystal shape and internal structure. Furthermore, changes in the X-ray diffraction pattern of trehalose dihydrate in the form of changes in peak width have been identified and have been attributed to microstructural changes due to crystallite size reduction and lattice deformations induced by milling during sample preparation.[30]

**Attenuated Total Reflection Fourier Transform Infrared Spectroscopy (ATR-FTIR).** ATR-FTIR spectra of trehalose dihydrate are characterized by relatively sharp absorption bands throughout the mid-IR region from 4000 to 900 cm$^{-1}$.[31,32] ATR-FTIR spectra of $T_{h1}$ and $T_{h2}$ (Figure 5) were in agreement with literature reports for $\alpha,\alpha$-trehalose dihydrate[31−37] and showed characteristic peaks at 3600−2800 cm$^{-1}$, 1650 cm$^{-1}$, and 1000−800 cm$^{-1}$ (see Table 1 for band assignments). These results show that although samples were generated via different methods, the resulting hydrogen bond arrangement (confirmed by ATR-FTIR results) were identical, thereby further confirming the identity of the two samples.

**Effect of Pan Type on Thermal Response: Conventional DSC.** The influence of pan type on the resultant thermal response of $\alpha,\alpha$-trehalose dihydrate (as well as the corresponding amorphous form)[12] is well documented.[10−13,38] In this study, the influence of pan type on the thermal behavior of both $T_{h1}$ and $T_{h2}$ was explored by conducting conventional DSC studies using pinholed and closed (i.e., crimped) pan systems.

Figure 6a illustrates the heating response for $T_{h1}$ DSC studies conducted at 2 °C/min using pinholed and closed pan systems. Pinholed experiments (solid line) saw a single endotherm at 97.2 °C (185.5 J/g) (similar to that identified previously by


dx.doi.org/10.1021/cg5004885 | Cryst. Growth Des. 2014, 14, 4955−4967

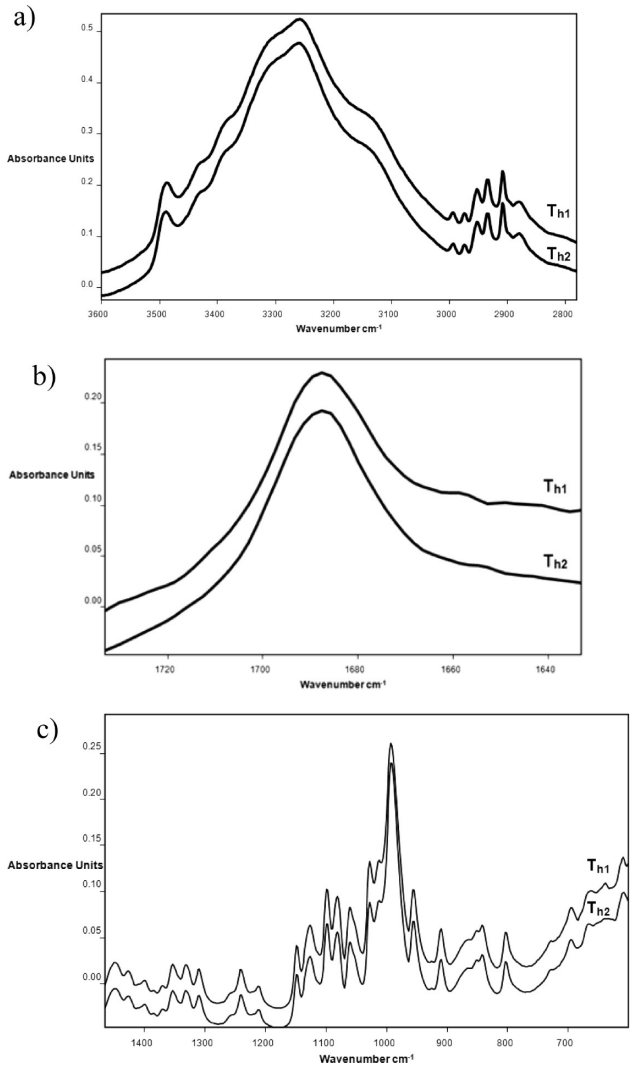


**Figure 5.** Expansions of the (a) 2800−3600 $cm^{-1}$, (b) 1660−1740 $cm^{-1}$, and (c) 600−1500 $cm^{-1}$ regions in the ATR-FTIR spectrum of $T_{h1}$ and $T_{h2}$ samples.

**Table 1. ATR-FTIR Band Assignment for Trehalose Dihydrate ($T_h$), $T_{h1}$, and $T_{h2}$ Samples**

| Absorption band ($cm^{-1}$) | | |
|---|---|---|
| $T_h$ | $T_{h1}$ and $T_{h2}$ | Assignment[11,30−36] |
| 3496 | 3488 | O−H stretch vibration of two crystal water molecules with Hydrogen bonding |
| 3269 | 3260 | |
| 3303 | 3294 | O−H stretching of trehalose |
| 2993 | 2995 | Asymmetrical and symmetrical stretching of the C−H ring |
| 2973 | 2973 | |
| 2950 | 2953 | |
| 2934 | 2934 | |
| 2907 | 2907 | |
| 2881 | 2879 | |
| 1685 | 1688 | Bending peak of crystal water |
| 994 | 992 | Two vibrational modes (asymmetrical and symmetrical) of the $\alpha,\alpha$-1↔1-glycosidic bond |
| 956 | 956 | |
| 924 | 925 | Coupled bending vibrations of C1−H, $CH_2$ and C−O−H |
| 911 | 911 | |
| 851 | 850 | Bending vibration of equatorial C−H bonds in $\alpha$ anomers |
| 842 | 840 | |

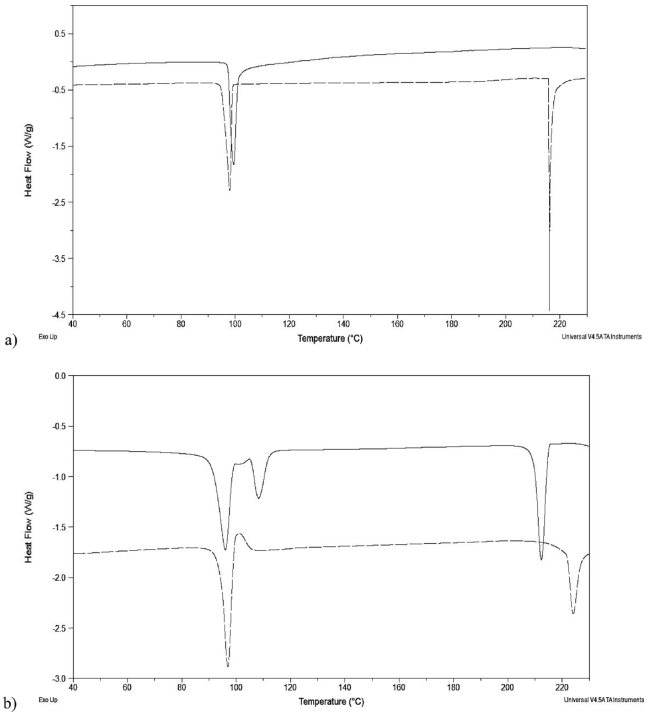


**Figure 6.** Conventional DSC (2 °C/min) response (data expressed in terms of heat flow) for (a) $T_{h1}$ and (b) $T_{h2}$ pinholed (solid line) and closed pan (dashed line) systems.

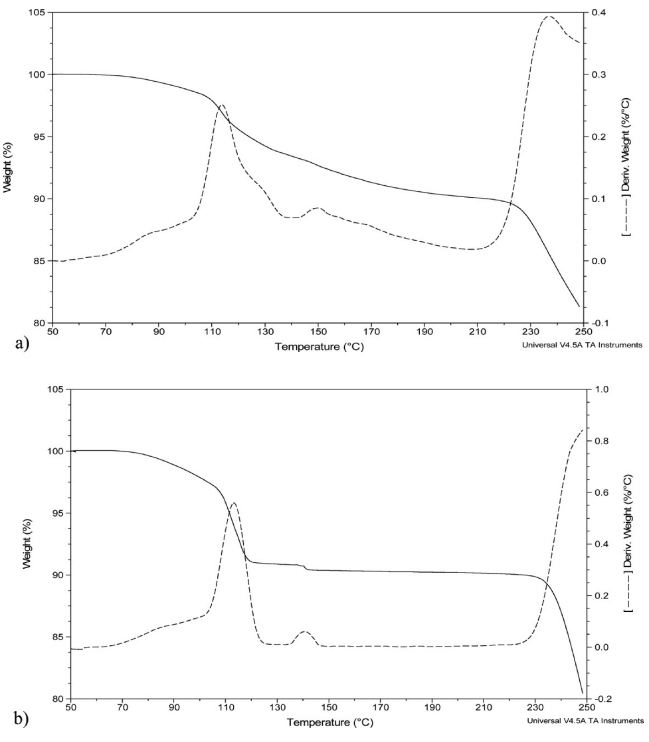


**Figure 7.** Typical TGA responses (2 °C/min, using pin-holed pan) for (a) $T_{h1}$ and (b) $T_{h2}$ (data expressed in terms of percentage weight and derivative weight).

Macdonald and Johari[16]), while closed pan (dashed line) experiments under the same experimental conditions saw the presence of two distinct endotherms; a first, reasonably broad endotherm at 94.9 °C (113.5 J/g) and the second sharper endotherm at 212.3 °C (113.8 J/g). These latter findings are


dx.doi.org/10.1021/cg5004885 | Cryst. Growth Des. 2014, 14, 4955−4967

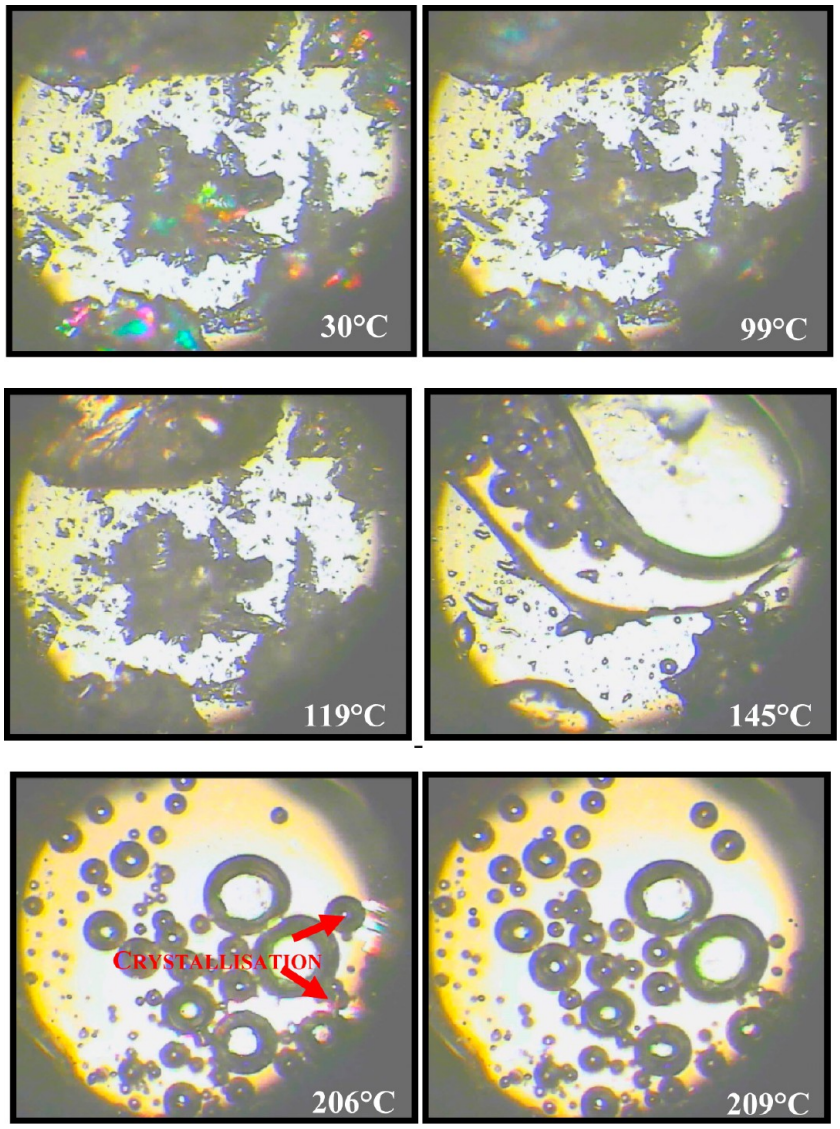


**Figure 8.** HSM images captured at specific temperatures for $T_{h1}$ sample heated at 2 °C/min.

similar to those observed by Shafizad and Susott[11] who, on heating trehalose dihydrate using closed pan systems, observed two sharp endotherms at 100 and 215 °C in their DSC studies. The first endotherm was attributed to the melt of the dihydrate and simultaneous formation of anhydrous crystals which melted at 215 °C.

Figure 6b shows the heating response for $T_{h2}$ samples. Pinholed experiments saw three different endotherms (similar to those identified by McGarvey et al.[12]) at 92.6 °C (144.5 J/g), 104.9 °C (32.4 J/g), and 209.8 °C (74.8 J/g). Closed pan experiments under the same experimental conditions saw two endotherms at 94.6 °C (119.8 J/g) and 215.2 °C (92.4 J/g), respectively. A crystallization exotherm was observed immediately after the first endotherm at 101.2 °C (31.7 J/g). In the literature,[5,10,11] this crystallization event (thought to be that of the stable anhydrate, $T_\beta$ which later melts at 215 °C) has been identified between 160 and 180 °C. The results presented in this study are in partial agreement with previous work,[5,10,11] the difference being that in this study, a crystallization exotherm was observed at ca. 100 °C.

Taken together, these data indicate first of all that the two batches show markedly different thermal responses. While overinterpretation of the peaks based on this data alone would not be appropriate, it is reasonable to suggest, based on reported literature,[3−6,9] that the $T_{h1}$ sample shows dehydration and melting, albeit with evidence of subsequent recrystallization to the stable anhydrate ($T_\beta$) for the closed pan systems, while $T_{h2}$ shows the formation of an intermediate ($T_\gamma$) which subsequently recrystallizes into the more stable solid anhydrate ($T_\beta$) which subsequently melts. It is well-known that the use of a closed pan system results in suppression of crystal water evaporation in the pan, therefore altering the equilibrium of the dehydration or evaporation process.[11,38,39] We suggest that the differences observed in this data set between the two batches may also be associated with the ease by which water may leave the sample, this being more a function of the differences in egress from the two powders themselves rather than the pan closure.

**Thermogravimetric Analysis (TGA).** TGA weight loss profiles (using pinholed pans) for $T_{h1}$ and $T_{h2}$ are shown in Figure 7a and b. Clear differences were observed between the two samples; these processes are shown in the derivative signal for clarity of events.


dx.doi.org/10.1021/cg5004885 | Cryst. Growth Des. 2014, 14, 4955−4967

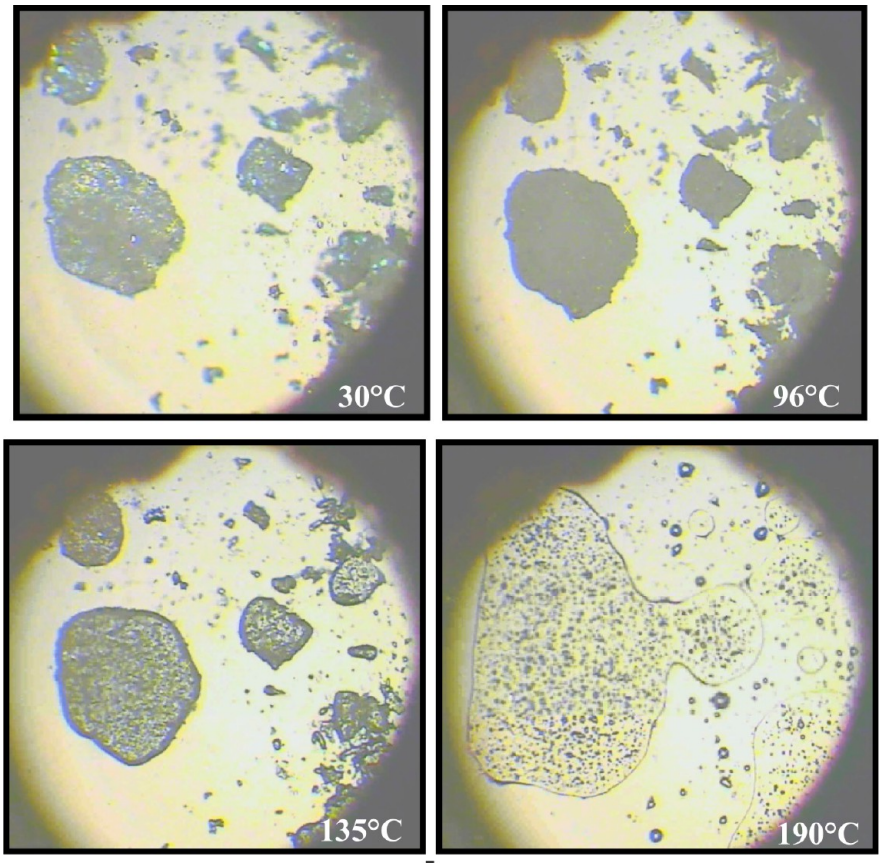


**Figure 9.** HSM images captured at specific temperatures for$T_{h2}$ sample heated at 2 °C/min.

No weight loss was evident below ca. 70 °C in both $T_{h1}$ and $T_{h2}$ samples. For $T_{h1}$ samples, a weight loss of 9.6% was observed between 70 and 200 °C, while for $T_{h2}$ samples, a weight loss of 9.6% was observed between 70 and 130 °C. All weight losses compared well within the limits to the expected 9.5% which equates to two molecules of water per molecule of trehalose.

There were, however, more marked differences in the temperature ranges over which the weight loss took place. $T_{h1}$ samples displayed an initial weight loss from ca. 70 to 110 °C (∼2%); this was followed by a second, more gradual decrease in weight from 110 to 200 °C (∼7.6%). In contrast, $T_{h2}$ samples demonstrated two distinct weight loss events (prior to the event at 230 °C which we ascribe to degradation) occurring at 70 °C (∼2.6%)and 105 °C (∼7%). It is apparent from these results that the rate of weight loss occurring in $T_{h2}$ samples is most rapid over the temperature range corresponding to the endotherms identified in DSC studies between 90 and 125 °C, linking them to the dehydration of the dihydrate crystal. There is clearly a question regarding how the DSC endotherms and the TGA weight loss profiles correspond, given the differences in experimental conditions. The sharpness of the DSC peaks would indicate structural breakdown which triggers, rather than represents, the water loss process which is energetically lower than the breaking of solid−solid bonds. Overall, the results clearly support the hypothesis that the two batches demonstrate significant differences in water egress profiles.

Previous work conducted by Mallet et al.[40] on large trehalose single crystals observed the nucleation and growth of vacuoles within these crystals using optical thermomicroscopy. Studies of trehalose single crystal dehydration (generated in the same manner as $T_{h1}$) by Berton et al.[29] confirmed the formation of vacuoles which occurred in the immediate vicinity of macroscopic crystal defects. On heating the crystals at 1 K/min from 90 to 120 °C (actual vacuole formation appeared to occur ∼102 °C), the authors observed the simultaneous progressive disappearance of these defects and the growth of the vacuoles which varied in diameter per crystal (10−200 $\mu$m) which were stable up to 200 °C.[29] Taking these observations into account, the more polycrystalline, and hence defect-rich, nature of $T_{h2}$ may be facilitating vacuole formation, leading to a facilitation of water loss and hence a more narrow temperature range over which water loss occurs.

**Hot-Stage Microscopy (HSM).** HSM studies were conducted on $T_{h1}$ and $T_{h2}$ samples at 2°/min, 30 to 250 °C, images are shown in Figures 8 and 9, respectively. $T_{h1}$ crystals were colored and showed birefringence at 30 °C (Figure 8). A change in birefringence was observed on heating commencing at ∼85 °C, continuing to ∼100 °C with crystals appearing darker and becoming more opaque (no melting observed) as observed in previous HSM studies of trehalose dihydrate and has been referred to as 'internal crystal modification'.[6,41] It has been proposed by Taylor and York[41] that the presence of bubbles below the crystal surface (which was seen in this study as crystals becoming darker) with increasing temperature suggests an impermeable layer of anhydrate formed around the bulk of the crystal, impeding water loss until the pressure generated by liberated hydrate water is sufficient to erupt through this layer. Further heating of $T_{h1}$ resulted in crystal melting, initiated at 118 °C in some crystals, with complete dissolution of all at 145 °C. Sussich et al.[6] have suggested that


dx.doi.org/10.1021/cg5004885 | Cryst. Growth Des. 2014, 14, 4955−4967

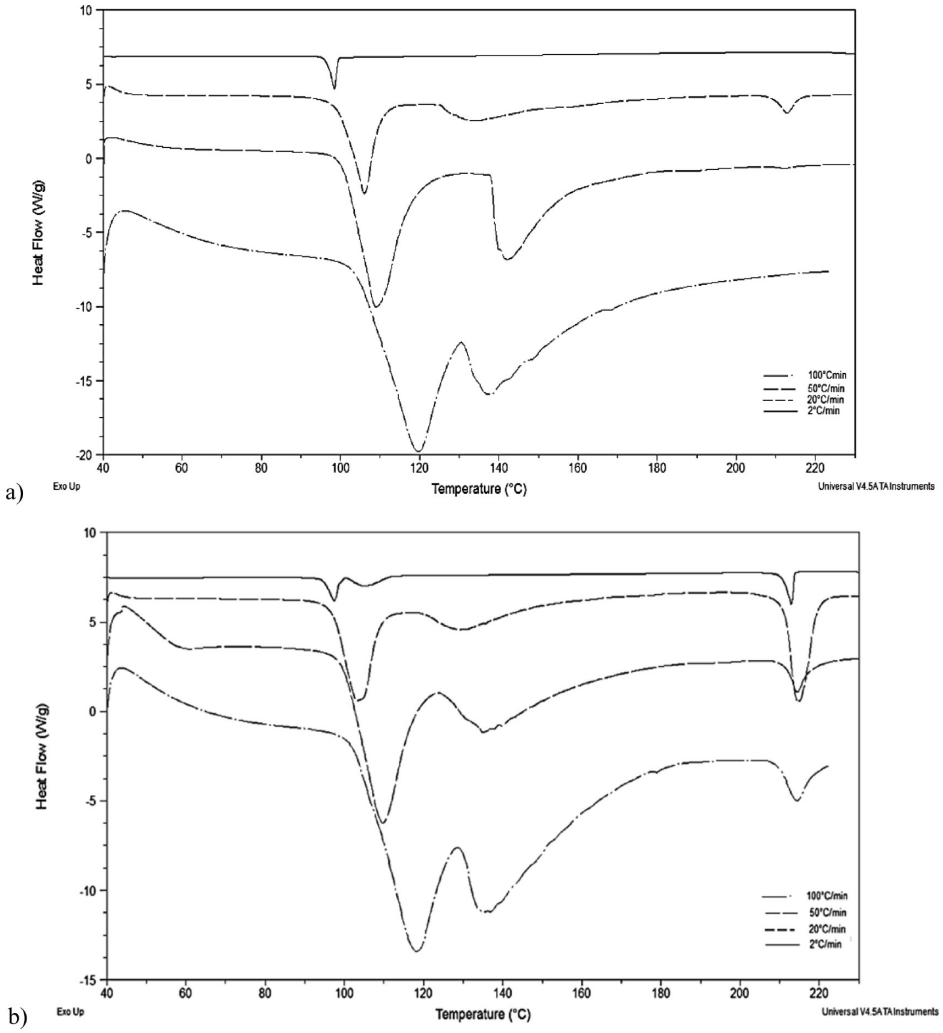


**Figure 10.** Conventional DSC (2, 20, 50, and 100 °C/min) response (data expressed in terms of heat flow) for (a) $T_{h1}$ and (b) $T_{h2}$ (pinholed pans used).

the melting of trehalose dihydrate (due to dehydration) produces an amorphous trehalose liquid which, on further heating, softens as the temperature exceeds its glass transition.[41] Further heating of $T_{h1}$ resulted in the production of small needle-like crystals, from 166 to 206 °C, which subsequently melted at 209 °C.

Heating the $T_{h2}$ samples (Figure 9) resulted in crystal melting (similar to $T_{h1}$), starting at 135 °C in some crystals with complete dissolution of all crystals at 190 °C. However, crystallization at high temperatures was not observed.

**Effect of Heating Rate on Thermal Response using Conventional DSC.** Both $T_{h1}$ and $T_{h2}$ were subjected to conventional DSC experiments using pinholed pans conducted at 2, 20, 50, and 100 °C/min (Figure 10). At high heating rates (i.e., 50 and 100 °C/min) experiments were not performed over 250 °C due to instrument limitations and cell contamination risks. DSC studies of $T_{h1}$ at 2 °C/min identified a single endotherm at 97.2 °C (185.5 J/g) (Figure 10a). At 20 °C/min, however, three endotherms were observed at 99.6 °C (124.5 J/g), 125.0 °C (76.2 J/g), and 208.4 °C (55.6 J/g). Two endotherms were observed at 50 °C/min and 100 °C/min at 101.30 °C (124.5 J/g), 132.52 °C (75.8 J/g) and 106.8 °C (76.5 J/g), 134.40 °C (57.0/g) respectively. Three endotherms were observed in $T_{h2}$ DSC studies conducted at 2, 20, 50, and 100 °C/min (Figure 10b). The onset temperatures appeared to shift with increasing heating rate for the first two endotherms, but not for the third endotherm which remained relatively constant at ca. 210 °C. Overall, the use of higher heating rates reduced the differences between the two samples, with both showing a double endotherm which has been previously associated with either the partial dehydration of the dihydrate followed by either further dehydration of $T_{\gamma}$[12] or the melt of the isomorph desolvate $T_{\alpha'}$[14] with both events resulting in the melt of the stable anhydrate $T_{\beta}$ (formed ca. 160−180 °C but not always detectable in DSC studies).

Slow heating conventional DSC studies using pinholed pans were conducted on $T_{h1}$ and $T_{h2}$ at 0.5, 1, and 2 °C/min with a focus on the first transitions seen as either one endotherm or two endotherms. A single endothermic peak (Figure 11) invariant with heating rate was observed at ca. 96 °C. $T_{h2}$ samples saw two broad low-temperature endothermic peaks also invariant with heating rate. The first endotherm was observed at 92.8 °C (142.0 J/g) (0.5 °C/min), 93.2 °C (141.9 J/g) (1 °C/min), and 95.1 °C (124.5 J/g) (2 °C/min) and appeared to shift slightly with increasing heating rate. The second endotherm was seen at ca. 102 °C.

Overall, the data have demonstrated that the differences between the two batches are seen most clearly at lower heating rates. While specific interpretation of all peaks is not possible, one may reasonably suggest that $T_{h2}$ shows a more complex


dx.doi.org/10.1021/cg5004885 | Cryst. Growth Des. 2014, 14, 4955−4967

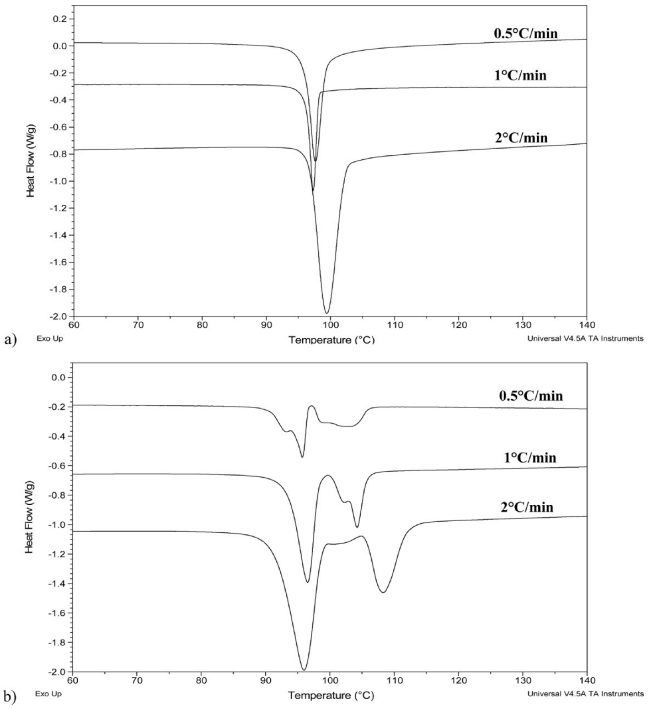


**Figure 11.** Conventional DSC (0.5, 1, and 2 °C/min) response (data expressed in terms of heat flow) for (a)$T_{h1}$ and (b)$T_{h2}$ (pinhole pans used).

thermal profile, particularly at slower heating rates, which suggests a greater range of transformation processes.

**Quasi-Isothermal MTDSC: Heat Capacity Measurements.** Quasi-isothermal MTDSC not only allows the equilibrium (or at least close to equilibrium) state of the system as a function of temperature to be observed, but also facilitates observation of the process by which that equilibrium is reached.[20] The temperature range at which the heat capacity alters significantly through a transition, indicating a kinetic component to the event can clearly be observed. Alternatively, the method allows the operator to monitor kinetic events by observing the change in reversing heat capacity as a function of time.[20]

In this study, quasi-isothermal MTDSC studies were conducted from 80 to 140 °C to characterize the transitions occurring within this temperature range without the influence of heating rate as observed in conventional DSC studies using fast and slow heating rates. A typical quasi-isothermal MTDSC trace for $T_{h1}$ and $T_{h2}$ showing the reversing heat capacity signal as a function of time is shown in Figure 12a. In both samples, between 80 and 100 °C, a discontinuity in the baseline was observed which appeared to be more complex in $T_{h2}$ samples. $T_{h1}$, however, showed a sudden increase in heat capacity at 96 °C suggestive of liquefaction. On further heating, evidence of slow solidification or slow crystallization was observed in both samples as confirmed by a decrease in the heat capacity. The final increase in heat capacity observed at ca. 120 °C in both samples suggests liquefaction, possibly of the solid form generated previously.

The data may also be expressed in terms of Lissajous figures (modulated heat flow as a function of time derivative of modulated temperature). Examples are plotted for $T_{h1}$ at 80 and 96 °C (Figure 12b) in order to analyze and draw conclusions from any changes observed compared with that observed in the reversing heat capacity signal. 80 °C was chosen as it was assumed (based on earlier findings) that at this temperature no thermal events occurred, while there may be time dependent events observed at 96 °C.

Both the axes of the Lissajous figures changed from 80 to 96 °C, reflecting changes in the heat capacity and phase angle of the response. Moreover, for the 96 °C sample there was clear time dependence, as indicated by the nonsuperimposition of the ellipses. The observed alterations in both heat capacity and time-dependence on holding temperature may reflect both changes in the water content of the system and alterations to the underlying crystal structure, both of which will result in changes to the heat capacity of the system.

Overall, therefore, the quasi-isothermal results are compatible with the DSC data in that they indicate a single major event for $T_{h1}$ samples while $T_{h2}$ shows a more complex reversing heat flow profile over a wide temperature range. Furthermore, Lissajous analysis indicates time dependence of the response for $T_{h1}$ at the beginning of the main thermal event, reflecting a decrease in heat capacity. We suggest that this is likely to reflect primarily water loss, as evidenced by both the time dependence of the response and the decrease in heat capacity, reflecting a reduction of the degrees of freedom within the system.

**Variable Temperature Attenuated Total Reflection Fourier Transform Infrared Spectroscopy (Variable Temperature ATR-FTIR).** In order to support the observations obtained via scanning thermal methods, FTIR studies were also conducted at a range of temperatures in order to identify structural changes to the samples on heating. Chemometric analysis (defined as applying multivariate statistical analysis techniques to chemical data[42]) was used in this study as a pattern recognition tool to distinguish between groups of spectra obtained during variable temperature ATR-FTIR studies. More specifically, hierarchical cluster analysis (HCA) and principle component analysis (PCA) were used to identify spectral changes occurring with increasing temperature which could be attributed to structural changes occurring in samples. HCA calculates and compares distances in spectral hyperspace between samples (or variables) in a data set. Data is presented as a dendrogram, where the length of a branch connecting two clusters relates to the similarity of the leaves within that cluster. The similarity is plotted on the top of the dendrogram, and a similarity value of 1 is assigned to identical samples while a value of 0 is assigned to the most dissimilar samples. A vertical line seen in a HCA dendrogram corresponds to the similarity value and partitions the dendrogram into distinguishable clusters.

PCA is a powerful visualization tool useful in variable temperature ATR-FTIR that finds linear combinations of original independent variables which account for maximal amounts of variation.[43] Scores analysis can be used to illustrate intersample relationships. Data is plotted as a two-dimensional (2D) scatter plot with a confidence ellipse superimposed. This ellipse represents a 95% confidence level derived from the score variance and is centered at the origin of the two score dimensions. In this study, all data points fell within the 95% confidence level (data not shown).

Variable temperature ATR-FTIR experiments were conducted on $T_{h1}$ and $T_{h2}$ samples at 2 °C/min from 30 to 198 °C (heating higher than 200 °C was not possible with the heating plate used); spectra were obtained at 1 min intervals. Figure 13a and b shows the variable temperature ATR-FTIR spectra of $T_{h1}$ and $T_{h2}$ showing two and three clusters as identified in HCA data (also shown), respectively.


dx.doi.org/10.1021/cg5004885 | Cryst. Growth Des. 2014, 14, 4955−4967

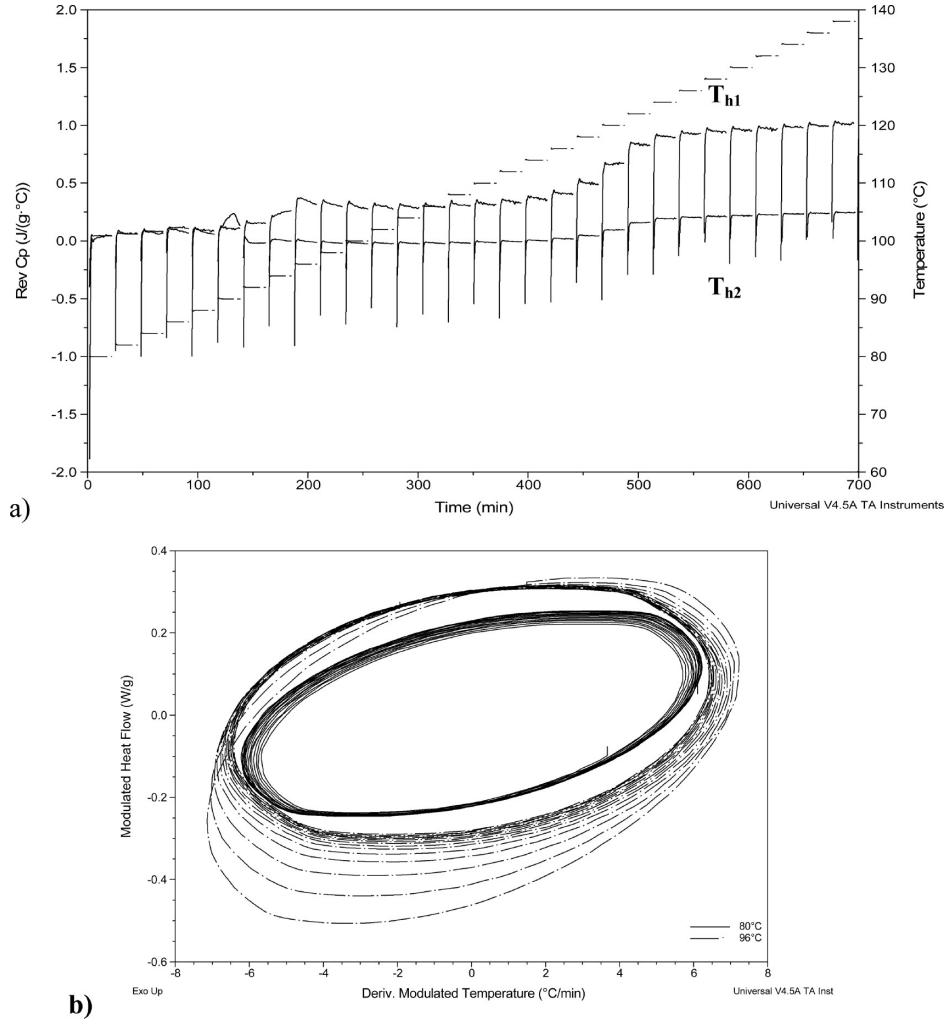


**Figure 12.** (a) Quasi-isothermal MTDSC reversing heat capacity (as a function of time) signal for $T_{h1}$ and $T_{h2}$. (b) Typical Lissajous figure in quasi-isothermal MTDSC as modulated heat flow (as a function of time derivative of modulated temperature) signal for $T_{h1}$ at 80 °C (solid line, inner set of ellipses) and 96 °C (dashed line, outer set of ellipses).

In $T_{h1}$ experiments (Figure 13a), the HCA dendrogram identified two clusters with a relatively low similarity value of approximately 0.3 indicating that samples identified within these clusters were relatively dissimilar. Analysis of the spectra showed that from 30 to 116 °C (depicted in red) $T_{h1}$ was crystalline as characterized by sharp absorption bands. At 118 °C spectra (depicted in black) changed and exhibited broad features which are an indication of a wide range of hydrogen bond lengths and orientations within the sample characteristic of an amorphous form. No further changes in the spectra were observed between 118 and 198 °C.

In $T_{h2}$ experiments (Figure 13b), the HCA dendrogram identified three clusters with a relatively low similarity value of approximately 0.22 indicating that samples identified within these clusters were comparatively dissimilar. Analysis of spectra obtained showed that from 30 to 116 °C (depicted in red) $T_{h2}$ was crystalline as characterized by sharp absorption bands in a similar trend to $T_{h1}$ samples. According to HCA, while still appearing to be crystalline in nature, the spectra obtained from 118 to 134 °C (depicted in green) differed from the spectra obtained from 30 to 116 °C (depicted in black). Finally, the spectra obtained from 136 to 198 °C exhibited broad features characteristic of an amorphous material (depicted in black).

Comparing the band assignments obtained to those in the literature, more specifically, in Raman and FTIR spectroscopy studies conducted on trehalose dihydrate by Gil et al.[35] and Dupray et al.,[13] spectra obtained at 124 °C in $T_{h2}$ samples showed characteristic bands of both the stable anhydrate ($T_\beta$) and the isomorphic desolvate ($T_\alpha$) (Form II and Form III,[35] respectively). Figure SI1 shows spectra obtained at 30, 118, 120, 124, and 130−138 °C (at 2 °C/min), while Table SI1 details the band assignment for $T_{h2}$ variable temperature ATR-FTIR spectra obtained at 124 °C for clarity.

Overall, Figures 12 and 13 clearly highlight spectral changes which occur on heating of both $T_{h1}$ and $T_{h2}$. The removal of the crystal water has great influence on the conformation and motional states of both samples as confirmed by the spectral changes observed at 118 °C. More specifically, further analysis of $T_{h2}$ spectra at 124 °C suggest that, on heating, $T_{h2}$ samples undergo structural rearrangement from the dihydrate to another crystalline material, which our ATR-FTIR data suggests to be a mixture of the stable and unstable anhydrate. This material undergoes amorphization at the lower temperatures. In contrast, $T_{h1}$ samples on heating undergo amorphization; however, further crystallization events are not observed on heating at higher temperatures.


dx.doi.org/10.1021/cg5004885 | *Cryst. Growth Des.* 2014, 14, 4955−4967

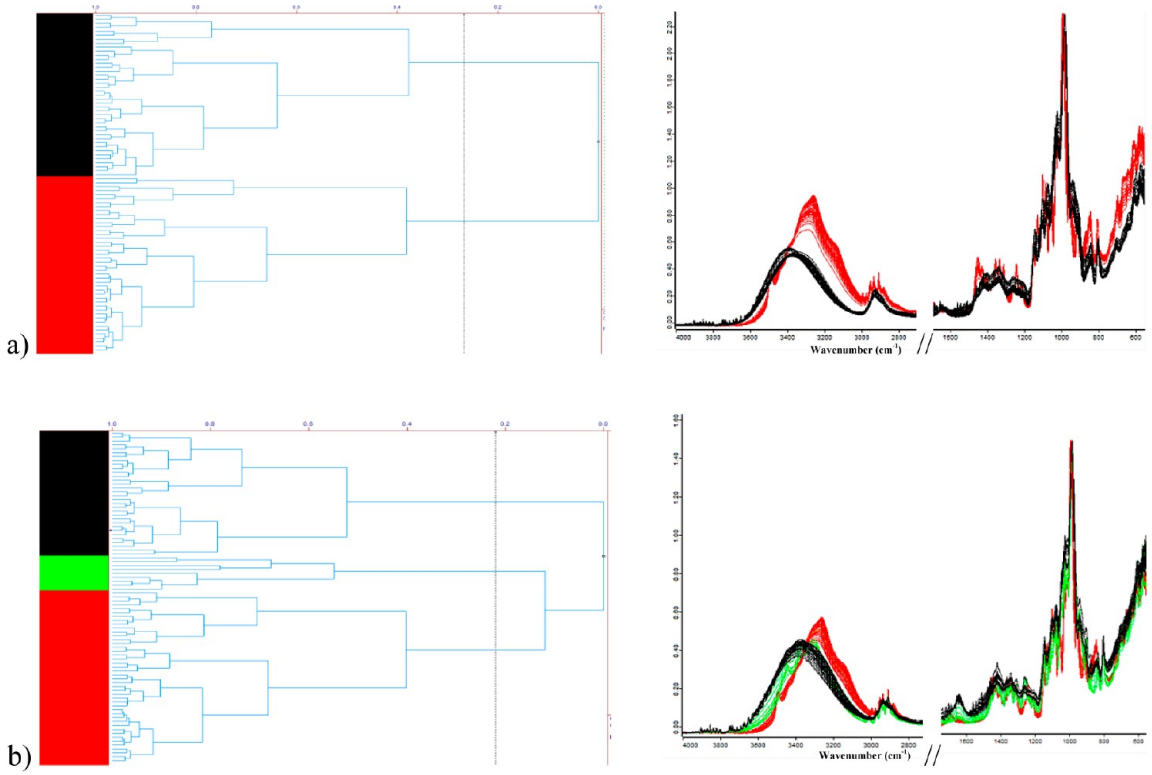


**Figure 13.** Variable temperature ATR-FTIR spectra of (a) $T_{h1}$ showing two clusters as identified in HCA data in the 600−1750 $cm^{-1}$ and 1000−4000 $cm^{-1}$ region (red spectra 30 to 116 °C, black spectra 118 to 198 °C); (b) $T_{h2}$ showing three clusters as identified in HCA data (red spectra 30 to 116 °C, green spectra 118 to 134 °C, black spectra 136 to 198 °C).

## DISCUSSION

The study has indicated that the generation of trehalose dihydrate via two routes (solvent evaporation and recrystallization from the amorphous state) results in material that is chemically and, from the viewpoint of unit cell structure, physically identical but which shows marked differences in both microstructure and thermal response. In terms of microstructure, the material recrystallized from the amorphous state ($T_{h2}$) showed a granular or defect-ridden appearance which we ascribe to the multiple nucleation associated with the recrystallization process, while the solvent-derived material ($T_{h1}$) shows a more continuous structure which we suggest reflects more growth rather than nucleation-dominated solidification process. In terms of the thermal response, examination of different scanning rates and pan types using DSC showed marked differences in endothermic and recrystallization profiles which may be related to previous work whereby the multiple peaks of individual batches have been studied, but the key to this study is the observation of differences in the water egress temperature range noted using TGA. In particular, the broader temperature range of water loss (but not weight loss total) for $T_{h1}$ is, we suggest, a reflection of the absence of multiple pathways for water loss from the continuous crystal structure. This hypothesis is supported by quasi-isothermal MTDSC which showed marked differences in heat capacity change with temperature for the two batches and with variable temperature ATR-FTIR which showed differences in temperature dependence of bond reconfiguration.

Overall, our study suggests that one possible mechanism for interbatch variation in trehalose dihydrate is differences in microstructure which in turn result in differences in water egress profiles. While it would not be appropriate to claim from these results alone that the frequently observed differences in behavior are solely due to this effect, it is noteworthy that the hypothesis does account for many of the observed interbatch incongruities such as the difficulty in establishing any difference between batches under ambient conditions, with differences manifesting on heating only.

## CONCLUSION

In this study, two standardized forms of trehalose dihydrate were generated by distinct methods in order to explore the mechanisms associated with interbatch variation. It was noted that the two routes resulted in differences in microstructure, with one batch ($T_{h2}$) showing a discontinuous formation with a granular or defect-ridden appearance, while the other ($T_{h1}$) showed a more continuous structure. Thermal studies indicated that the DSC traces differed considerably, as has been previously noted for different batches, while studies on water loss patterns as a function of temperature indicated that there were significant differences in the ease of egress, with $T_{h2}$ showing weight loss over a much more narrow temperature range even though the total amount of water lost was the same for both batches. We introduce the technique of quasi-isothermal MTDSC within the field, which again showed marked differences in temperature dependent heat capacity which we ascribe to differences in water loss profiles. Variable temperature ATR FTIR spectroscopy indicated differences in temperature-dependent bond profiles commensurate with differing water release characteristics. Overall, the study has shown that the differences in the two batches generated may be ascribed to differences in water loss profiles which we suggest is associated with microstructure, with the granular structure of $T_{h2}$ facilitating water loss more than the more structurally continuous $T_{h1}$.


dx.doi.org/10.1021/cg5004885 | *Cryst. Growth Des.* 2014, 14, 4955−4967

## ■ ASSOCIATED CONTENT

### Supporting Information

Variable temperature ATR-FTIR spectra (Figure SI1) and band assignment (Table SI1) of $T_{h2}$ samples at 124 °C. This material is available free of charge via the Internet at http://pubs.acs.org.

## ■ AUTHOR INFORMATION


### Corresponding Author

*E-mail: duncan.craig@ucl.ac.uk.


### Author Contributions

The manuscript was written through contributions of all authors. All authors have given approval to the final version of the manuscript. All authors contributed equally.

### Notes

The authors declare no competing financial interest.

## ■ ACKNOWLEDGMENTS


The authors would like to thank Mr. Bertrand Leze (School of Environmental Sciences, University of East Anglia) for his assistance with the JEOL JSM 5900LV Scanning Electron Microscope and the Thermo-Arl-Xtra Powder X-ray Diffractometer.


## ■ REFERENCES


(1) Cesàro, A.; De Giacomo, O.; Sussich, F. Water interplay in trehalose polymorphism. *Food Chem.* **2008**, *106* (4), 1318−1328.

(2) Verhoeven, N.; Neoh, T. L.; Furuta, T.; Yamamoto, C.; Ohashi, T.; Yoshii, H. Characteristics of dehydration kinetics of dihydrate trehalose to its anhydrous form in ethanol by DSC. *Food Chem.* **2012**, *132* (4), 1638−1643.

(3) Reisener, H. J.; Goldschmid, H. R.; Ledingham, G. A.; Perlin, A. S. Formation of trehalose and polyols by wheat stem rust (Puccinia graminis tritici) uredospores. *Can. J. Biochem. Physiol.* **1962**, *40*, 1248−1251.

(4) Nagase, H.; Endo, T.; Ueda, H.; Nakagaki, M. An anhydrous polymorphic form of trehalose. *Carbohydr. Res.* **2002**, *337*, 167−173.

(5) Furuki, T.; Kishi, A.; Sakurai, M. De- and rehydration behavior of alpha,alpha-trehalose dihydrate under humidity-controlled atmospheres. *Carbohydr. Res.* **2005**, *340* (3), 429−438.

(6) Sussich, F.; Urbani, R.; Princivalle, F.; Cesaro, A. Polymorphic amorphous and crystalline forms of trehalose. *J. Am. Chem. Soc.* **1998**, *120* (31), 7893−7899.

(7) Sussich, F.; Princivalle, F.; Cesaro, A. The interplay of the rate of water removal in the dehydration of alpha,alpha-trehalose. *Carbohydr. Res.* **1999**, *322* (1−2), 113−119.

(8) Pyszczynski, S. J.; Munson, E. J. Generation and characterization of a new solid form of trehalose. *Mol. Pharmaceutics* **2013**, *10* (9), 3323−3332.

(9) De Giacomo, O. Z. *Molecular Mobility of Trehalose in Relation to its Bioprotective Action*; University of Trieste, 2008.

(10) Sussich, F.; Bortoluzzi, S.; Cesaro, A. Trehalose dehydration under confined conditions. *Thermochim. Acta* **2002**, *391* (1−2), 137−150.

(11) Shafizad, F.; Susott, R. A. Crystalline transitions of carbohydrates. *J. Org. Chem.* **1973**, *38* (21), 3710−3715.

(12) McGarvey, O. S.; Kett, V. L.; Craig, D. Q. M. An investigation into the crystallization of alpha,alpha-trehalose from the amorphous state. *J. Phys. Chem. B* **2003**, *107* (27), 6614−6620.

(13) Dupray, V.; Berton, B.; Ossart, S.; Atmani, H.; Petit, M. N.; Coquerel, G. Concomitant dehydration mechanisms in single crystals of alpha,alpha-trehalose. *Carbohydr. Res.* **2009**, *344* (18), 2539−2546.

(14) Taylor, L. S.; York, P. Effect of particle size and temperature on the dehydration kinetics of trehalose dihydrate. *Int. J. Pharm.* **1998**, *167* (1−2), 215−221.

(15) Horvat, M. Effect of Particle Size on Physico-chemical Properties on Trehalose-Paracetmol mixture; Masters thesis; University of Zagreb, Zagreb, Croatia, 2003.

(16) Macdonald, C.; Johari, G. P. Glass-softening of trehalose and calorimetric transformations in its liquid state. *J. Mol. Struct.* **2000**, *523*, 119−132.

(17) Armstrong, C. L.; Forbes, R. T.; Blair, J.; York, P. Thermal behaviour of alpha,alpha-trehalose dihydrate batches. *Eur. J. Pharm. Sci.* **1996**, *4* (SUPPL), S181.

(18) Wunderlich, B.; Jin, Y.; Boller, A. Mathematical description of differential scanning calorimetry based on periodic temperature modulation. *Thermochim. Acta* **1994**, *238* (0), 277−293.

(19) Kaneko, H.; Osada, T.; Iijima, M. Quasi-isothermal measurement by TMDSC in isotactic polypropylene. *J. Therm. Anal. Calorim.* **2008**, *92* (3), 807−811.

(20) Lai, H. L.; Pitt, K.; Craig, D. Q. M. Characterisation of the thermal properties of ethylcellulose using differential scanning and quasi-isothermal calorimetric approaches. *Int. J. Pharm.* **2010**, *386* (1−2), 178−184.

(21) Manduva, R.; Kett, V. L.; Banks, S. R.; Wood, J.; Reading, M.; Craig, D. Q. M. Calorimetric and spatial characterization of polymorphic transitions in caffeine using quasi-isothermal MTDSC and localized thermomechanical analysis. *J. Pharm. Sci.* **2008**, *97* (3), 1285−1300.

(22) Qi, S.; Craig, D. Q. M. The development of modulated, quasi-isothermal and ultraslow thermal methods as a means of characterizing the $\alpha$ to $\gamma$ indomethacin polymorphic transformation. *Mol. Pharmaceutics* **2012**, *9* (5), 1087−1099.

(23) Thomas, L.; Aubuchon, S. Heat capacity measurements using quasi-isothermal MDSC; TA Instruments, Thermal Analysis & Rheology, 1997.

(24) Verdonck, E.; Schaap, K.; Thomas, L. C. A discussion of the principles and applications of Modulated Temperature DSC (MTDSC). *Int. J. Pharm.* **1999**, *192* (1), 3−20.

(25) Wunderlich, B. Quasi-isothermal temperature-modulated differential scanning calorimetry (TMDSC) for the separation of reversible and irreversible thermodynamic changes in glass transition and melting ranges of flexible macromolecules. *Pure Appl. Chem.* **2009**, *81*, 1931−1952.

(26) Jiang, Z.; Imrie, C. T.; Hutchinson, J. M. Temperature modulated differential scanning calorimetry. Part III. Effect of heat transfer on phase angle in quasi-isothermal ADSC. *Thermochim. Acta* **1999**, *336* (1−2), 27−40.

(27) Kawakami, K.; Ida, Y. Application of modulated-temperature DSC to the analysis of enantiotropically related polymorphic transitions. *Thermochim. Acta* **2005**, *427* (1−2), 93−99.

(28) Lammert, A. M.; Schmidt, S. J.; Day, G. A. Water activity and solubility of trehalose. *Food Chem.* **1998**, *61* (1−2), 139−144.

(29) Berton, B.; Dupray, V.; Atmani, H.; Coquerel, G. Gas vacuoles formation during the dehydration of trehalose dihydrate: A Raman microspectroscopy approach. *J. Therm. Anal. Calorim.* **2007**, *90* (2), 325−328.

(30) Willart, J. F.; Dujardin, N.; Dudognon, E.; Danède, F.; Descamps, M. Amorphization of sugar hydrates upon milling. *Carbohydr. Res.* **2010**, *345* (11), 1613−1616.

(31) Wolkers, W. F.; Oliver, A. E.; Tablin, F.; Crowe, J. H. A Fourier-transform infrared spectroscopy study of sugar glasses. *Carbohydr. Res.* **2004**, *339* (6), 1077−1085.

(32) Akao, K.; Okubo, Y.; Asakawa, N.; Inoue, Y.; Sakurai, M. Infrared spectroscopic study on the properties of the anhydrous form II of trehalose. Implications for the functional mechanism of trehalose as a biostabilizer. *Carbohydr. Res.* **2001**, *334* (3), 233−241.

(33) Kacuráková, M.; Mathlouthi, M. FTIR and laser-Raman spectra of oligosaccharides in water: characterization of the glycosidic bond. *Carbohydr. Res.* **1996**, *284* (2), 145−157.

(34) Wolkers, W. F.; Oldenhof, H.; Alberda, M.; Hoekstra, F. A. A Fourier transform infrared microspectroscopy study of sugar glasses: application to anhydrobiotic higher plant cells. *Biochim. Biophys. Acta* **1998**, *1379* (1), 83−96.

(35) Gil, A. M.; Belton, P. S.; Felix, V. Spectroscopic studies of solid alpha-alpha trehalose. *Spectrochim. Acta, Part A* **1996**, *52* (12), 1649−1659.
(36) Belton, P. S.; Gil, A. M. IR and Raman spectroscopic studies of the interaction of trehalose with hen egg white lysozyme. *Biopolymers* **1994**, *34* (7), 957−961.
(37) Lin, S.-Y.; Chien, J.-L. In vitro simulation of solid-solid dehydration, rehydration, and solidification of trehalose dihydrate using thermal and vibrational spectroscopic techniques. *Pharm. Res.* **2003**, *20* (12), 1926−1931.
(38) Taylor, L. S.; York, P. Characterization of the phase transitions of trehalose dihydrate on heating and subsequent dehydration. *J. Pharm. Sci.* **1997**, *87* (3), 347−355.
(39) Craig, D. Q.; Reading, M. *Thermal analysis of pharmaceuticals*; CRC press: 2010.
(40) Mallet, F.; Petit, S.; Coquerel, G. *BIWIC 11*; 2004; Vol. *190*.
(41) Taylor, L. S.; York, P. Characterization of the phase transitions of trehalose dihydrate on heating and subsequent dehydration. *J. Pharm. Sci.* **1998**, *87* (3), 347−355.
(42) Dai, X.; Moffat, J. G.; Wood, J.; Reading, M. Thermal scanning probe microscopy in the development of pharmaceuticals. *Adv. Drug Delivery Rev.* **2012**, *64* (5), 449−460.
(43) Grisedale, L. C.; Moffat, J. G.; Jamieson, M. J.; Belton, P. S.; Barker, S. A.; Craig, D. Q. M. Development of photothermal FTIR microspectroscopy as a novel means of spatially identifying amorphous and crystalline salbutamol sulfate on composite surfaces. *Mol. Pharmacol.* **2013**, *10* (5), 1815−1823.